Multi-order phononic frequency comb generation within a MoS2 electromechanical resonator

Anis Chiout, Franck Correia, Meng-Qiang Zhao, A T Charlie Johnson, Debora Pierucci, Fabrice Oehler, Abdelkarim Ouerghi, Julien Chaste

Applied Physics Letters

Multi-order phononic frequency comb generation within a MoS_2 electromechanical resonator

Cite as: Appl. Phys. Lett. **119**, 173102 (2021); https://doi.org/10.1063/5.0059015
Submitted: 04 June 2021 • Accepted: 19 September 2021 • Published Online: 25 October 2021

Anis Chiout, Franck Correia, Meng-Qiang Zhao, et al.

AIP Publishing

Applied Physics Letters ARTICLE scitation.org/journal/apl

Multi-order phononic frequency comb generation within a MoS_2 electromechanical resonator

Cite as: Appl. Phys. Lett. **119**, 173102 (2021); doi: 10.1063/5.0059015
Submitted: 4 June 2021 · Accepted: 19 September 2021 ·
Published Online: 25 October 2021

View Online Export Citation CrossMark

Anis Chiout,[1] Franck Correia,[1] Meng-Qiang Zhao,[2,3] A. T. Charlie Johnson,[3] Debora Pierucci,[1] Fabrice Oehler,[1] Abdelkarim Ouerghi,[1] and Julien Chaste[1,a)]

AFFILIATIONS

[1]Université Paris-Saclay, CNRS, Centre de Nanosciences et de Nanotechnologies, 91120 Palaiseau, France
[2]Department of Physics and Astronomy, University of Pennsylvania, 209S 33rd Street, Philadelphia, Pennsylvania 19104 6396, USA
[3]Department of Chemical and Materials Engineering, New Jersey Institute of Technology, 138 Warren Street, Newark, New Jersey 07103, USA

[a)]Author to whom correspondence should be addressed: julien.chaste@universite-paris-saclay.fr

ABSTRACT

In this work, we measure and tune simultaneously the vibration of a 1-nm thick MoS_2 suspended monolayer with standard electrical excitation and optical techniques. At ambient temperature, we first investigate the strong parametric coupling between two different mechanical modes (ω_1 and ω_2). We demonstrate a high and quasi-linear tunability of the mode frequencies with the parametric pump voltage. Then, we couple the highly tunable main vibration (ω_1) to a parametric pump frequency (ω_p) to obtain a high number of sidebands at frequencies $\omega_1 \pm m\,\omega_p$, driving the mechanical mode with a large external electrical force. This oscillating force, applied via the gate voltage, acts as a stress onto the MoS_2 sheet. The obtained frequency comb has a large spectral band and contains up to 100 harmonics, with potential applications in quantum information processing and heat or sound transport.

Among all the different classes of mechanical resonators, from levitated nanoparticles[1] to Lirgo-Virgo interferometers,[2] carbon nanotubes and membranes made of two-dimensional (2D) atomically thin materials are characterized by very low mass (m)[3,4] and stiffness constants (k).[5] This specificity has been used to fabricate the best external mass and force detectors.[3,6] In these resonators, the classical Hooke's law that defines the relation between force and elongation, $F = k.\Delta x$, displays a strongly tunable spring constant. Given that the intrinsic value of k is globally small, the linear elasticity force applied to the membrane is often negligible compared to external forces. In our experiment, the effect of the external electrostatic capacitive force dominates the mechanical frequency spectrum $\omega = \sqrt{k/m}$ through k variation. Driven using a simple gate voltage, our suspended membrane resonators can achieve ~100% efficient frequency tunability (few MHz/V) for a main resonance vibrating in the tens of MHz.[4,7] This extreme tunable range is about two orders of magnitude higher than other typical resonators (1% of frequency).

When a pump signal is applied to a mechanical system, parametric amplification phenomena can occur, as in carbon nanotube,[8] graphene,[9,10] or MoS_2[11] nanoresonators or even thermal noise squeezing.[6,12,13] When parametric amplification is performed with extreme tunability over multiple mechanical resonances, it is possible to create mechanical systems with strong and coherent coupling between several resonances.[14–16] In this situation, energy transfer between modes by coherent Rabi oscillations has already been measured.[16–18]

An important objective in phonons engineering is to obtain the mechanical analogue of an optical frequency comb, for which the resulting spectrum is a sum of periodic resonances separated by the parametric pump frequency over a wide bandwidth (i.e., more than an octave). Until now, experimental realizations have been limited to coupling with the first harmonics of the pump signal (with total number of harmonics $M = 4$).[17,19–23] Building on the particular properties of our particular 2D material resonator, we first demonstrate the efficient coupling of two simple mechanical modes, and then we couple a single mode to the external electrostatic pump to obtain a large number of harmonics, up to $M = 100$. Our findings may enable coherent phonon manipulation that would be useful for quantum information processing,[17,24–26] sensors,[27] phonon laser-like,[28–30] or innovative concepts in heat and sound transports.[31]

Previously,[32] we have fabricated resonators using large suspended MoS_2 membranes (~100 μm) deposited on pre-patterned silicon

oxide/Si substrates with gold metallic contacts, see Fig. 1(a). The etching of patterns in the oxide allows one to design arbitrary geometries of suspended membranes. In this study, we deposited a monolayer of MoS_2 onto an array of silicon oxide pillars. The MoS_2 was obtained by chemical vapor deposition on a Si substrate and transferred by wet etching to the pillar array (KOH solution assisted by polymethyl methacrylate, PMMA).[33] All mechanical and optical measurements are performed in vacuum (1×10^{-5} mbar) at room temperature (~300 K). Our specific experimental setup allows us to monitor simultaneously the resonance by dual electrical and optical methods. This combination enables one to evaluate the mechanical response of the membrane in a simple way, detailed as follows. First, an electrostatic force F activates the vertical motion of the membrane with a potential difference (gate voltage) applied between the membrane and the substrate. Then, the cavity formed by the 2D membrane and the Si substrate acts as a Fabry–Pérot interferometer, which modulates the reflection of the laser probe (633 nm). After interference, the laser intensity depends on the length of the cavity, which is directly the vertical position of the MoS_2 membrane, relative to the Si surface. We measure the reflected laser (~10 μW) with a photodetector (APD130A Thorlab) and a lock-in (Zurich instr.). Such optical interferometric measurements are very precise and allow for the optical quantification of the membrane displacement at room temperature. From previous measurements,[32,34] we estimate a typical quality factor of ~150 of the main mechanical resonance (at 300 K). This particular setup can, thus, benchmark the quality of our fabricated resonator, without any intrusive or destructive external probe. It is important to note that no optical or electrical heating builds up during our measurements,[32] which are conducted using a low laser power of 10 μW. Figure 1(b) shows the mechanical response of the suspended material driven at frequency $f_D = \omega_D/2\pi$. In all our measurements, the amplitude of the motion corresponds to the voltage measured on the lock-in in mV without any correction factor. We define z the displacement of the membrane relative to its rest position. The geometry is a MoS_2 monolayer deposited on a SiO_2 pillars array. These pillars are made to obtain multiple resonators in a single sample. The pillars have 230 nm of radius and 440 nm of height. The backgate-MoS_2 distance is 660 nm. These pillars are made to obtain multiple resonators in a single sample. Some resonators consist of a square membrane delimited by 4 pillars at the corners and some by a matrix of 3×3 pillars where the pillar in the middle is missing, which we approximate by circular membrane of 5 μm diameter. We have confirmed this approximation in our previous report.[32] We observe multiple resonances, which correspond to the different vibration modes of the same resonator. We note $f_1 = \omega_1/2\pi$ and $f_2 = \omega_2/2\pi$ the two main resonances: f_1 corresponds to the fundamental mode (n,m) = (0,1) of the modeled circular membrane, and f_2 to a higher mode.

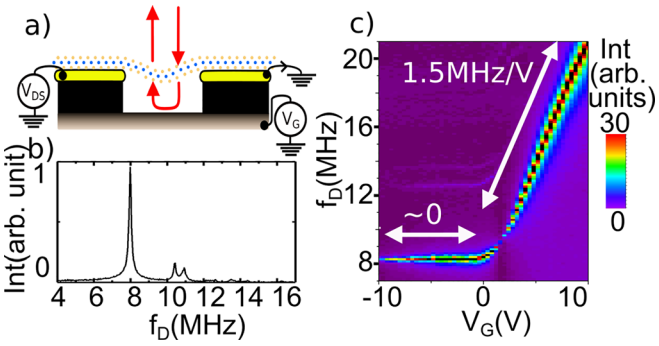

FIG. 1. Optoelectromechanical system of a suspended monolayer of MoS_2. (a) A schematic of the suspended sample with electrical transistor configuration and optomechanical measurements. (b) Mechanical resonance f_1 as a function of the drive frequency f_D applied to the gate. (c) The gate voltage dependence of the mechanical frequency is atypical and strongly asymmetric. The region of interest for parametric pumping, above few volts, shows a quasi linear dependence with $\delta f_D/\delta V_G \approx 1.5\,\text{MHz V}^{-1}$.

The measurement of the gate dependence of f_1 is shown in Fig. 1(c). Below a certain threshold voltage around $V_G = 0$ V, the mode frequency remains constant. On the contrary, above a few volts of gate voltage, f_1 is almost linearly tunable with the gate voltage. Similar behavior is observed for f_2 (not shown). Such a tunable range covers approximately 12 MHz, which corresponds to more than 100% tunability (f_1= 8 MHz) using electrical tension mediated stress. This important specificity is key to implement tunable parametric pumping experiments with our nanomechanical resonators.

If we push to larger gate voltages, we recover the standard $|V_G|$ or V_G^2 dependence from capacitive forces, and the symmetry of the system is restored, with resonance shift for negative V_G values ($V_G < -15$ V), see the supplementary material. In practice, such behavior can be modeled by a standard external force $F = C'\Delta V_G^2$,[34] where $C' = dC/dz$ with C being the capacitance and ΔV_G being the potential difference along the gate, $\Delta V_G = V_G - \Phi + V_P.\cos(\omega_P t) + V_D.\cos(\omega_D t)$. V_P,V_D, ω_D, and ω_P are the pump and drive oscillating voltage amplitude and frequency, respectively. In the probed V_G range [−10 V, 10 V], we see an additional perturbation to the capacitive force; the observed asymmetry may relate to the specifics of our geometry (pillars array), or to a transverse polarization V_{DS} creating a non-uniform electric field[35] or to persistent charge trapping, as demonstrated by the strong persistent photocurrent in our MoS_2 layers.[34] Note that other measurements (see the supplementary material) on circular drums, a more conventional geometry, do not present such asymmetry, which highlights the role of the particular arrayed geometry used in this work.

In Fig. 2, we now fix the gate voltage at $V_G = 4$ V, in the linear highly tunable domain. Using $V_{ds} = 5$ V, we measure $\omega_1 = 2\pi \times 12.2$ MHz and $\omega_2 = 2\pi \times 16.7$ MHz. Then, we apply an additional pump voltage V_P over the gate voltage at frequency $f_P = \omega_P/2\pi$. The phase difference between the two signals is fixed at 0°. Since the mechanical mode frequencies f_i are dynamically tunable, the corresponding k_i will be modulated at ω_P. We define the mode difference $\Delta\omega = \omega_2 - \omega_1$. In Fig. 2(a), we plot the evolution of the mechanical response against the pump frequency. At the peculiar point where the pump frequency f_p matches the mode frequency difference, $\omega_P = \Delta\omega = 4.5$ MHz, we observe a strong anti-crossing, which is the signature of an efficient inter-mode coupling. In addition, many resonances appear around the main peak at $f_1 \pm m \times f_P$, where m is an integer. By analogy with the Stokes and anti-Stokes resonances, we attribute these peaks to intra-mode coupling between the first mechanical mode (f_1) and the harmonics of the pump (f_p). Considering the observed intra- and inter-mode couplings, we can model the mechanical system by a set of two coupled vibrations modes, as described by Okamoto *et al.*[17] In this framework, the motion equations are defined as follows:

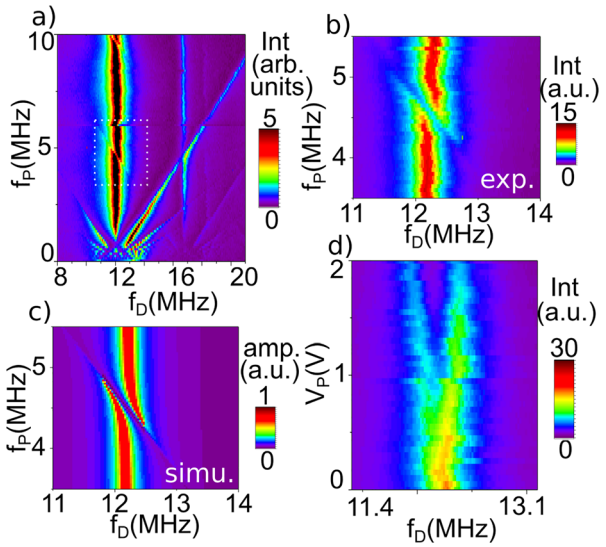

FIG. 2. Mechanical coupling between two modes at $f_1 = 12.2$ MHz and $f_2 = 16.7$ MHz: (a) amplitude vertical motion as a function of the pump frequency f_p and drive frequency f_D at $V_G = 4$ V, $V_{ds} = -5$ V, $V_D = 10$ mV, and $V_P = 1.5$ V. A first anti-crossing is observable when $f_p = 5$ Mhz $\approx f_2 - f_1$. Another crossing can be seen at $f_p = 9.5$ MHz between f_1 and $f_3 = 22$ MHz. (b) Zoom on the first anti-crossing at smaller drive voltage ($V_D = 1$ mV). (c) Corresponding simulation with mode coupling parameter $c = 2\pi \times 4.632$ MHz. (d) Main mode splitting as a function of V_P and drive frequency f_D ($V_D = 1$ mV, $f_p = 4.5$ MHz).

$$\begin{cases} \ddot{x_1} + \gamma_1\dot{x_1} + \left({\omega_1}^2 + \Gamma_+.\cos(\omega_P t)\right)x_1 + \Lambda.\cos(\omega_P t)x_2 \\ \quad = F_1.\cos(\omega_D t + \varphi) \\ \ddot{x_2} + \gamma_2\dot{x_2} + \left({\omega_2}^2 + \Gamma_-.\cos(\omega_P t)\right)x_2 + \Lambda.\cos(\omega_P t)x_1 \\ \quad = F_2.\cos(\omega_D t + \varphi) \end{cases} \quad (1)$$

We define x_1 (x_2) as the motion amplitude for the mode ω_1 (ω_2) with the damping rate γ_1 (γ_2) driven by a force F_1 (F_2). The Γ_+ and Γ_- coefficients are related to the tunability Γ of the mode with the pump frequency defined as $\Gamma = \omega\times(\delta\omega/\delta V_P)\times V_P$ with $\delta\omega/\delta V_P$ the voltage-controlled frequency detuning ($\delta\omega/\delta V_P = 2\pi\times 1.5$ MHz V^{-1} in our experiment). In this framework, we have $\Gamma_\pm = \Gamma\left(1 \pm \omega_1\Delta\omega/\sqrt{c^2 + {\omega_1}^2\Delta\omega^2}\right)$, where Λ represents the amplitude of coupling between modes, $\Lambda = \Gamma\left(c/2\sqrt{c^2 + {\omega_1}^2\Delta\omega^2}\right)$, and c is the mode coupling parameter. The corresponding simulation in Fig. 2(c) confirms that the model given in Eq. (1) reproduces with great accuracy the anti-crossing with coupling constant $\Lambda \sim c = (2\pi \times 4.632\,\text{MHz})^2$.

The mode frequency splitting (2g) at the anti-crossing point between the two modes is shown in Fig. 2(d) as a function of V_P. At $V_P = 1.5$ V, the frequency splitting value is $2g = 350$ kHz, which corresponds to the expected theoretical value of $2g = \Lambda/\left(2\sqrt{\omega_1\omega_2}\right)$.[9,17] This mode frequency splitting value is very large compared to previous reports,[9,11,16] which explains the preservation of the anti-crossing at room temperature even if the mechanical quality factor is average ($Q = 150$).

Next, we turn to focus on the complex intra-mode coupling observed in the lower half of Fig. 2(a) ($f_p < 3$MHz). A low frequency but very high amplitude pump excitation is used to generate a frequency comb pattern. In Fig. 3(a), we use a high pump voltage ($V_P = 4$ V) at a location where the resonance tunability is completely turned-off [$V_G = -10$ V, see Fig. 1(b)]. Although the pump voltage is high, the pump excitation has little effect on the main mode frequency. Conversely, Fig. 3(b) explores the high tunability regime ($V_G = 4$ V) at the same pump voltage ($V_P = 4$ V). There, we observe many Stokes and anti-Stokes generations, resulting in the appearance of a large frequency comb-like spectrum between 8 and 20 MHz. We observe multiple anti-crossing (blue/green area) all along the probed spectral window. We interpret this effect as the collective interference of all the different m-order components generated by the pump and their respective main mode.

This picture is within the scope of the theory proposed by Okamoto *et al.*,[17] and we can use the same theoretical tools to simulate our data, as shown in Fig. 3(c). The theoretical amplitude variations

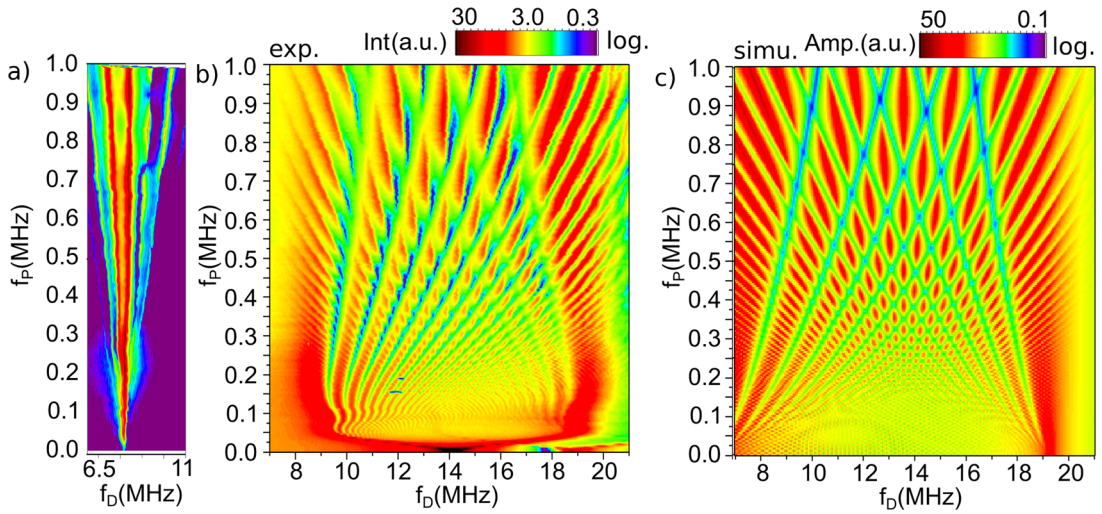

FIG. 3. Low frequency pump regime and strong coupling of the intermode: (a) and (b) vertical motion amplitude as a function of f_p and f_D for a high pump amplitude of $V_P = 4$ V at $V_G = -10$ V and $V_G = 4$ V, i.e., for different voltage-controlled frequency detuning of $\approx$0 MHz V^{-1} and $\approx$1.5 MHz V^{-1}, respectively. (c) The simulation of the intramode coupling with $\Lambda = 0$.

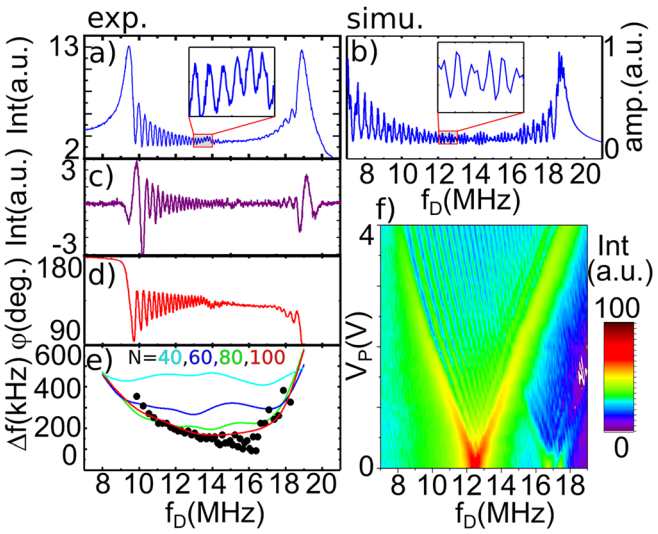

FIG. 4. Very high harmonic number (M = 100) for the intramode coupling and high pump amplitude. (a) Experimental variation of the amplitude signal as a function of the drive when f_p = 75 kHz ($\delta\omega_1/\delta V_P$) = 2π 1.5 MHz V^{-1} and (b) simulation with, in inset, the zoom on few oscillation. The mechanical response to a high pump drive is an oscillating signal between 8 and 18 MHz. In (c), the same signal with a background subtraction, and in (d), the phase. (e) The black dot shows the frequency period between each oscillation as a function of the drive frequency. The color lines show the oscillating period number for different harmonic. M = 100 is required to fit our data. (f) The pump drive dependence of the output signal with f_p = 150 kHz.

are in good agreement with the observed experiment. Phase variations (shown in supplementary material) also show a good match between experiment and theory with the intramode coupling parameter $\Gamma_1 = 2\pi \times 12.7$ MHz.[2] As shown so far, room-temperature is not detrimental in all our experiments, and we are capable of maintaining a high coherence, with huge number of sidebands (up to M = 100). The present observations let us think that the energy transfer rate is higher than the dissipation rate.

By introducing slowly varying m-th harmonic idler amplitudes, $a_m(t) = a_m e^{i\omega_P.m.t}$ with m positive or negative integers, we can expand $x_1(t)$ and $x_2(t)$ as Fourier sum of these amplitudes. Neglecting the $a''_m(t)$ term and the intermode coupling ($\Lambda = 0$), we obtain the following equation set:

$$(2i(\omega + m\omega_P) + \gamma_1)\dot{a_m} + \left(-(\omega + m\omega_P)^2 + i\gamma_1(\omega + m\omega_P) + {\omega_1}^2\right)a_m + \Gamma_1/2.a_{m+1} + \Gamma_1/2.a_{m-1} = F_1.e^{i\delta}.\delta_{m,0}. \quad (2)$$

The number of equations is determined by the number (2M + 1) of pump harmonic m used in the calculation, $-M \le m \le M$. In order to determine the highest harmonic index M, we look at the spectral profile for a small f_p with [Figs. 4(a) and 4(b)] and without [Fig. 4(c)] background signal. Compared to Fig. 3(b), the frequency resolution has been improved. The vertical motion amplitude varies rapidly as a function of the driving frequency, and there are as many oscillations as jumps in the phase plot [see Fig. 4(d) and the supplementary material, Fig. S2]. Calculations for f_p = 75 kHz, Fig. 4(b), match the measurements. By measuring the frequency difference between adjacent oscillations (Δf) as a function of the drive frequency f_d, we can estimate a value of M. Black dots in Fig. 4(e) indicate the experimental frequencies difference as a function of ω_D. Compared to simulations with increasing harmonic number M, the position of the experimental data demonstrates that we need at least M = 100 in order to match the observed frequency spacing.

In Fig. 4(f), we measure the frequency response as a function of the pump voltage. The appearance of multiple resonances and harmonics for high parametric pumping has been observed. The density of the peaks increases with V_P, and therefore, frequency spacing Δf decreases, which suggests an increase in M with increasing pump voltage V_P. From this observation, we can get a physical meaning for the observed high value of M. The pump signal is a low frequency voltage oscillation centered on a constant V_G. Via the strong linear tunability, the main mode frequency, thus, repeatedly sweeps the same frequency interval. During the measurement shown in Fig. 4(a), the resonator sweeps a frequency window Δf_W = 11 MHz (from 8 to 19 MHz) in 6.5 μs (half period of 75 kHz). This duration is slightly faster than the resonator damping rate ($\sim 11\mu$s) and the decoherence time. During this time, the resonator is coherently coupled with almost all of the pump harmonic contained in Δf_W. We can obtain a rough estimate of the highest index of harmonics using $\Delta f_W/f_P$ = 147 for f_P = 75 kHz [Fig. 1(e)]. The computed value of M $\sim$ 100 [Fig. 4(e)] is, thus, consistent with the above estimate.

Based on this encouraging result, future experiments may be able to measure the temporal response of pulsed burst probes. In this way, we could explore other non-linear responses of the oscillator, such as electromechanically induced transparency or Fano-like resonances.

To conclude, we have fabricated a highly tunable mechanical resonator using a suspended MoS_2 monolayer with gate and side contacts. By combining electrical and optical measurements, we demonstrate the existence of strong mechanical inter-mode coupling at room temperature. Using the highly linear tunability of our resonator, we highlight the efficient coupling between a parametric pump and the main mechanical mode. We obtain a mechanical response shaped as frequency comb, which spans over an octave. The required number of harmonics to simulate the data is in excess of 100, which is 25-time higher than previous measurements.[17] Thanks to this large number of high-frequency modes, this suspended MoS_2-based resonator is of great interest for applications in nano-opto-electromechanics (NOEMS).[32]

See the supplementary material for additional measurements of the frequency dependence at larger gate voltages, phase measurements of the intramode coupling, and I(V) curves of the fabricated device.

We thank Remy Braive for his help during the set-up of the optical experiment. This work was supported by French grants ANR ANETHUM (No. ANR-19-CE24-0021) and ANR Deus-nano (No. ANR-19-CE42-0005) and by the French Renatech network. M.Q.Z. acknowledges the support from NJIT Start-up Funds.

AUTHOR DECLARATIONS

Conflict of Interest

The authors have no conflicts to disclose.

DATA AVAILABILITY

The data that support the findings of this study are available from the corresponding author upon reasonable request.

REFERENCES

[1]G. Ranjit, M. Cunningham, K. Casey, and A. A. Geraci, Phys. Rev. A **93**, 053801 (2016).
[2]LIGO Scientific Collaboration and Virgo Collaboration *et al.*, Phys. Rev. Lett. **116**, 061102 (2016).
[3]J. Chaste, A. Eichler, J. Moser, G. Ceballos, R. Rurali, and A. Bachtold, Nat. Nanotechnol. **7**, 301 (2012).
[4]C. Chen, S. Rosenblatt, K. I. Bolotin, W. Kalb, P. Kim, I. Kymissis, H. L. Stormer, T. F. Heinz, and J. Hone, Nat. Nanotechnol. **4**, 861 (2009).
[5]M. K. Blees, A. W. Barnard, P. A. Rose, S. P. Roberts, K. L. McGill, P. Y. Huang, A. R. Ruyack, J. W. Kevek, B. Kobrin, D. A. Muller, and P. L. McEuen, Nature **524**, 204 (2015).
[6]P. Weber, J. Güttinger, A. Noury, J. Vergara-Cruz, and A. Bachtold, Nat. Commun. **7**, 12496 (2016).
[7]A. Eichler, J. Moser, J. Chaste, M. Zdrojek, I. Wilson-Rae, and A. Bachtold, Nat. Nanotechnol. **6**, 339 (2011).
[8]A. Eichler, J. Chaste, J. Moser, and A. Bachtold, Nano Lett. **11**, 2699 (2011).
[9]J. P. Mathew, R. N. Patel, A. Borah, R. Vijay, and M. M. Deshmukh, Nat. Nanotechnol. **11**, 747 (2016).
[10]Z.-J. Su, Y. Ying, X.-X. Song, Z.-Z. Zhang, Q.-H. Zhang, G. Cao, H.-O. Li, G.-C. Guo, and G.-P. Guo, arXiv:1909.13219 [Cond-Mat, Physics:Physics] (2020).
[11]P. Prasad, N. Arora, and A. K. Naik, Nanoscale **9**, 18299 (2017).
[12]R. D. Alba, F. Massel, I. R. Storch, T. S. Abhilash, A. Hui, P. L. McEuen, H. G. Craighead, and J. M. Parpia, Nat. Nanotechnol. **11**, 741 (2016).
[13]R. Singh, R. J. T. Nicholl, K. I. Bolotin, and S. Ghosh, Nano Lett. **18**, 6719 (2018).
[14]A. Eichler, M. del, Á. Ruiz, J. A. Plaza, and A. Bachtold, Phys. Rev. Lett. **109**, 025503 (2012).
[15]S. S. P. Nathamgari, S. Dong, L. Medina, N. Moldovan, D. Rosenmann, R. Divan, D. Lopez, L. J. Lauhon, and H. D. Espinosa, Nano Lett. **19**, 4052 (2019).
[16]P. Prasad, N. Arora, and A. K. Naik, Nano Lett. **19**, 5862 (2019).
[17]H. Okamoto, A. Gourgout, C.-Y. Chang, K. Onomitsu, I. Mahboob, E. Y. Chang, and H. Yamaguchi, Nat. Phys. **9**, 480 (2013).
[18]D. Zhu, X.-H. Wang, W.-C. Kong, G.-W. Deng, J.-T. Wang, H.-O. Li, G. Cao, M. Xiao, K.-L. Jiang, X.-C. Dai, G.-C. Guo, F. Nori, and G.-P. Guo, Nano Lett. **17**, 915 (2017).
[19]M. Park and A. Ansari, in *2018 IEEE International Frequency Control Symposium (IFCS)* (IEEE, 2018), pp. 1–4.
[20]A. Ganesan, C. Do, and A. Seshia, Appl. Phys. Lett. **112**, 021906 (2018).
[21]D. A. Czaplewski, C. Chen, D. Lopez, O. Shoshani, A. M. Eriksson, S. Strachan, and S. W. Shaw, Phys. Rev. Lett. **121**, 244302 (2018).
[22]A. Ganesan and A. Seshia, Sci. Rep. **9**, 9452 (2019).
[23]L. S. Cao, D. X. Qi, R. W. Peng, M. Wang, and P. Schmelcher, Phys. Rev. Lett. **112**, 075505 (2014).
[24]Y. Chu, P. Kharel, W. H. Renninger, L. D. Burkhart, L. Frunzio, P. T. Rakich, and R. J. Schoelkopf, Science **358**, 199 (2017).
[25]J. Bochmann, A. Vainsencher, D. D. Awschalom, and A. N. Cleland, Nat. Phys. **9**, 712 (2013).
[26]J. D. Teufel, T. Donner, D. Li, J. W. Harlow, M. S. Allman, K. Cicak, A. J. Sirois, J. D. Whittaker, K. W. Lehnert, and R. W. Simmonds, Nature **475**, 359 (2011).
[27]S. Kolkowitz, A. C. B. Jayich, Q. P. Unterreithmeier, S. D. Bennett, P. Rabl, J. G. E. Harris, and M. D. Lukin, Science **335**, 1603 (2012).
[28]R. M. Pettit, W. Ge, P. Kumar, D. R. Luntz-Martin, J. T. Schultz, L. P. Neukirch, M. Bhattacharya, and A. N. Vamivakas, Nat. Photonics **13**, 402 (2019).
[29]I. S. Grudinin, H. Lee, O. Painter, and K. J. Vahala, Phys. Rev. Lett. **104**, 083901 (2010).
[30]J. Zhang, B. Peng, ŞK. Özdemir, K. Pichler, D. O. Krimer, G. Zhao, F. Nori, Y. Liu, S. Rotter, and L. Yang, Nat. Photonics **12**, 479 (2018).
[31]M. Maldovan, Nature **503**, 209 (2013).
[32]J. Chaste, A. Missaoui, S. Huang, H. Henck, Z. Ben Aziza, L. Ferlazzo, C. Naylor, A. Balan, A. T. C. Johnson, Jr.,, and R. Braive, and others. ACS Nano **12**, 3235 (2018).
[33]C. De-Eknamkul, X. Zhang, M.-Q. Zhao, W. Huang, R. Liu, A. T. C. Johnson, and E. Cubukcu, 2D Mater. **7**, 014004 (2019).
[34]J. Chaste, I. Hnid, L. Khalil, C. Si, A. Durnez, X. Lafosse, M.-Q. Zhao, A. T. C. Johnson, S. Zhang, J. Bang, and A. Ouerghi, ACS Nano **14**, 13611 (2020).
[35]Q. P. Unterreithmeier, E. M. Weig, and J. P. Kotthaus, Nature **458**, 1001 (2009).